Naval Research Laboratory
Washington, DC 20375-5320

NRL/8224/MR—2023/1

A Comparison of Finite-Rate Chemistry and Flamelet Generated Manifold Approaches in a Premixed Cavity Stabilized Combustor

CAL J. RISING

Fluids Systems Section
Spacecraft Engineering Division

GABRIEL B. GOODWIN

Hypersonic Aerodynamics and Propulsion Section
Spacecraft Engineering Division

April 4, 2023

REPORT DOCUMENTATION PAGE

Form Approved
OMB No. 0704-0188

1. REPORT DATE *(DD-MM-YYYY)*	**2. REPORT TYPE**	**3. DATES COVERED** *(From - To)*
04-04-2023	NRL Memorandum Report	

4. TITLE AND SUBTITLE

A Comparison of Finite-Rate Chemistry and Flamelet Generated Manifold Approaches in a Premixed Cavity Stabilized Combustor

5a. CONTRACT NUMBER

5b. GRANT NUMBER

5c. PROGRAM ELEMENT NUMBER

6. AUTHOR(S)

Cal J. Rising and Gabriel B. Goodwin

5d. PROJECT NUMBER

5e. TASK NUMBER

5f. WORK UNIT NUMBER
6C11

7. PERFORMING ORGANIZATION NAME(S) AND ADDRESS(ES)

Naval Research Laboratory
4555 Overlook Avenue, SW
Washington, DC 20375-5320

8. PERFORMING ORGANIZATION REPORT NUMBER

NRL/8220/MR--2023/1

9. SPONSORING / MONITORING AGENCY NAME(S) AND ADDRESS(ES)

Naval Research Laboratory
4555 Overlook Avenue, SW
Washington, DC 20375-5320

10. SPONSOR / MONITOR'S ACRONYM(S)

NRL 6.2 Base Program

11. SPONSOR / MONITOR'S REPORT NUMBER(S)

12. DISTRIBUTION / AVAILABILITY STATEMENT

DISTRIBUTION STATEMENT A: Approved for public release; distribution is unlimited.

13. SUPPLEMENTARY NOTES

14. ABSTRACT

Numerical simulations of combustor physics can become prohibitively expensive when a detailed mechanism is utilized to model the reactions and intermediate species production. Flamelet models are able to avoid this issue by pre-calculating the chemistry using simplified 0D or 1D calculations and tabulating the results to be interpolated into the 3D simulations. In the current study, Reynolds Averaged Navier-Stokes simulations are performed on the University of Virgina Supersonic Combustion Facility (UVASCF) using a 32 species, 206 reaction ethylene-air skeletal mechanism using both finite-rate chemistry (FRC) and a flamelet generated manifold (FGM). The simulations are performed on the same mesh and using identical boundary conditions to identify the influence of the chemistry modeling approach on the solution. The results demonstrate differences in the species distribution for the FGM methodology as the CH_2O production is more diffuse and OH production is more stratified. The outflow characteristics are compared to each other and are revealed to be in reasonable agreement while the computational cost for the FGM method decreased by approximately 32x as compared to the cost with FRC.

15. SUBJECT TERMS

16. SECURITY CLASSIFICATION OF:			**17. LIMITATION OF ABSTRACT**	**18. NUMBER OF PAGES**	**19a. NAME OF RESPONSIBLE PERSON**
					Cal Rising
a. REPORT	**b. ABSTRACT**	**c. THIS PAGE**	U	18	**19b. TELEPHONE NUMBER** *(include area code)*
U	U	U			(202) 404-1253

Standard Form 298 (Rev. 8-98)
Prescribed by ANSI Std. Z39.18

This page intentionally left blank.

CONTENTS

FIGURES

TABLES

This page intentionally left blank

EXECUTIVE SUMMARY

Numerical simulations of combustor physics can become prohibitively expensive when a detailed mechanism is utilized to model the reactions and intermediate species production. Flamelet models are able to avoid this issue by pre-calculating the chemistry using simplified 0D or 1D calculations and tabulating the results to be interpolated into the 3D simulations. In the current study, Reynolds Averaged Navier-Stokes simulations are performed on the University of Virgina Supersonic Combustion Facility (UVASCF) using a 32 species, 206 reaction ethylene-air skeletal mechanism using both finite-rate chemistry (FRC) and a flamelet generated manifold (FGM). The simulations are performed on the same mesh and using identical boundary conditions to identify the influence of the chemistry modeling approach on the solution. The results demonstrate differences in the species distribution for the FGM methodology as the CH_2O production is more diffuse and OH production is more stratified. The outflow characteristics are compared to each other and are revealed to be in reasonable agreement while the computational cost for the FGM method decreased by approximately 32x as compared to the cost with FRC.

This page intentionally left blank

A COMPARISON OF FINITE-RATE CHEMISTRY AND FLAMELET GENERATED MANIFOLD APPROACHES IN A PREMIXED CAVITY STABILIZED COMBUSTOR

1. INTRODUCTION

Increased knowledge of the flow-field dynamics within dual mode scramjet engines is vital for the continued development of hypersonic flight vehicles. It is necessary for the engines within these vehicles to have stable and efficient combustion across a variety of flight conditions [1]. However, operating at high flight speeds presents challenges in flame stability due the fluid dynamic timescales being larger than the chemical reaction time scales [2]. This has led to the use of cavity flameholders to generate a low-speed recirculation zone which increases residence time and improves fuel-air mixing [3–5]. In addition, cavity flameholders are advantageous due to their low pressure and drag penalties when compared to other flameholding devices [3]. Therefore, there is a need to fully understand the flame and flow interactions within cavity combustors to further develop high speed propulsion vehicles.

The University of Virginia Supersonic Combustion Facility (UVASCF) dual-mode direct-connect combustor displayed in Figure 1, is used to study premixed ethylene air combustion at condition up to a flight Mach of 5. The facility has had numerous experimental studies which have characterized the cavity-stabilized flame and the corresponding velocity field. Previous research by Kirik et. al. utilized particle image velocimetry and planar laser-induced fluorescence to quantify the flame and flow within the cavity [6]. Additionally, Cutler et. al. performed coherent anti-Stokes Raman spectroscopy measurements to quantify the species concentrations and temperature under reacting conditions [7]. These experimental studies have provided the characteristic boundary conditions and flame-flow behavior which can be used to validate further numerical simulation studies.

Several numerical studies have been completed in the UVASCF to further examine the performance of the facility under subsonic combustion conditions. A series of Hybrid Reynolds-Averaged Navier Stokes/Large Eddy Simulations (RANS/LES) were performed to simulate combustion within the UVASCF [8–10]. These studies performed a full tip-to-tail simulation of the facility and showed reasonable agreement with experimental velocimetry and flame measurements. Nielsen et. al. determined that it is necessary to accurately capture the inflow turbulence and flame angle to properly predict the shock-train within the isolator [10]. Additionally, detailed investigations of the combustion processes within the cavity using Discontinuous Galerkin Large Eddy Simulations have been performed [11–13]. Goodwin et. al. highlighted the impact of inflow turbulence intensity into the cavity and its influence on the the vortex shedding and correspondingly the flame structure [13].

The prior numerical studies have all relied on higher fidelity flow solvers such as LES or hybrid LES/RANS which can be prohibitively expensive when simulating full experimental facilities and reacting flows due to the required grid resolution and detailed chemistry models. In this paper, we present RANS simulations of premixed ethylene-air combustion in the UVASCF to compare the RANS approach to the

Manuscript approved April 2, 2023.

previous results to assess the ability of the a lower fidelity approach to capture the average reacting flow-field. The simulations are performed using finite-rate chemistry (FRC) and a flamelet-generated manifold (FGM) approach is utilized to examine the effects of a reduced order chemistry approach. The results of each chemistry modeling approach are compared to each other to evaluate the accuracy and computational cost.

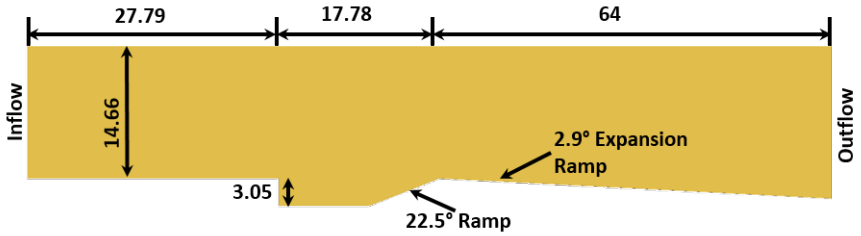

Fig. 1—Geometry of UVASCF combustor. All units are in mm.

2. NUMERICAL METHODS

In this study the multi-component chemically reacting Reynolds-Averaged Navier Stokes equations are solved, which are defined as

$$\frac{\partial \rho}{\partial t} + \nabla \cdot (\rho \overline{\boldsymbol{v}}) = 0 \tag{1}$$

$$\frac{\partial (\rho \overline{\boldsymbol{v}})}{\partial t} + \nabla \cdot (\rho \overline{\boldsymbol{v}} \otimes \overline{\boldsymbol{v}}) = -\nabla \cdot \overline{p}_{mod} \mathbb{I} + \nabla \cdot (\overline{\boldsymbol{T}} + \boldsymbol{T_{RANS}}) \tag{2}$$

$$\frac{\partial \left(\rho \overline{E}\right)}{\partial t} + \nabla \cdot (\rho \overline{E} \overline{\boldsymbol{v}}) = -\nabla \cdot \overline{p}_{mod} \overline{\boldsymbol{v}} + \nabla \cdot (\overline{\boldsymbol{T}} + \boldsymbol{T_{RANS}}) \overline{\boldsymbol{v}} \tag{3}$$

$$\frac{\partial \left(\rho \boldsymbol{Y_i}\right)}{\partial t} + \nabla \cdot (\rho U \boldsymbol{Y_i}) = \nabla \cdot (\boldsymbol{J_i} + \frac{\mu_t}{Sc_t} \nabla \boldsymbol{Y_i}) \tag{4}$$

where ρ is density, $\overline{\boldsymbol{v}}$ is the mean velocity, p_{mod} is the modified mean pressure, $\mathbb{I}$ is an identity matrix, $\overline{\boldsymbol{T}}$ is the mean viscous stress tensor, $\boldsymbol{T_{RANS}}$ is the Reynolds stress tensor, $\overline{\boldsymbol{E}}$ is the mean total energy, $\boldsymbol{Y_i}$ is the mass fraction of the species, $\boldsymbol{J_i}$ the diffusive flux, μ_t is the turbulent viscosity, and σ_t is the turbulent Schmidt number. Pressure is determined using the ideal gas law as the equation of state.

To close out the Reynolds Stress tensor the two equation SST k-ω turbulence model is used. This turbulence model solves transport equations for the turbulent kinetic energy and specific dissipation rate.

The turbulence model was modified by Menter to include a blending function to effectively combine a k-ω model in the boundary layer and a k-ϵ model away from the wall [14]. This turbulence model has been successfully implemented in previous cavity stabilized simulations and has been shown to produce results which agree with experimental results [15–17].

2.1 Reacting Flow Modeling

The reacting flow is solved using two separate approaches to compare the results from each. The first method is the finite rate chemistry approach that directly solves the species transport equation, which is given as

$$\frac{\partial}{\partial t}\rho \boldsymbol{Y_i} + \frac{\partial}{\partial x_j}(\rho u_j \boldsymbol{Y_i} + F_{k,j}) = \omega_i \tag{5}$$

where $\boldsymbol{F_{k,j}}$ is the diffusion flux component and ω_i is the rate of production of the ith species. This can result in an increased computational expense when it comes to using detailed mechanisms which have many intermediate species and reactions.

The second method is a Flamelet-Generated Manifold where the thermo-chemistry is tabulated and parameterized by mixture fraction, heat loss ratio, and progress variable. The manifold is generated using the governing equations for a 1D premixed strained reactor which solves the opposed flow premixed flame equations in progress variable space at a fixed mixture fraction. The equations are as follows:

$$\frac{\partial Y_i}{\partial \tau} = (X_c)\frac{\partial^2 Y_i}{\partial c^2} + \frac{\dot{\omega}_i}{\rho} - \frac{\partial Y_i}{\partial t}\frac{\dot{\omega}_i}{\rho} \tag{6}$$

$$\frac{\partial T}{\partial \tau} = \frac{X_c}{C_p}\left(\frac{\partial C_p}{\partial c} + \sum_{i=1}^{N} C_p \frac{\partial Y_i}{\partial c}\right)\frac{\partial T}{\partial c} + X_c\frac{\partial^2 T}{\partial c^2} - \frac{1}{\rho C_p}\sum_{i=1}^{N} h_i \dot{\omega}_i - \frac{\partial T}{\partial c}\frac{\dot{\omega}_c}{\rho} \tag{7}$$

where τ is the pseudo-time, C_p is the heat capacity, h_i is the enthalpy of the ith species, $\dot{\omega}_i$ is the reaction rate of the ith species, and $\dot{\omega}_c$ is the progress variable reaction rate. The equations are integrated in pseudo-time until the unsteady terms have reached a value which is less than a specified tolerance. The progress variable is defined as the progress of the reaction occurring and is mathematically represented as

$$y = \sum (W_k Y_k) \tag{8}$$

$$c = \frac{y - y_u}{y_b - y_u} \tag{9}$$

where y is the progress variable of the mixture, c is the normalized progress variable, y_u is the progress variable of the unburnt initial state, and y_b is the progress variable at the burnt state. The progress variable Favre averaged transport equation is

$$\frac{\partial \rho y}{\partial t} + \nabla \cdot (\rho u y) - \nabla \cdot (\Gamma_y \nabla y) = \dot{\omega_y} \tag{10}$$

where $\dot{\omega_y}$ is the progress variable source term and Γ_y is the diffusivity computed from the material properties of the mixture. To solve for the progress variable source term, the turbulent flame speed closure (TFC) model is selected which assumes the reaction occurs in a thin layer which separates the reactants and products with the mean reaction rate being closed by the turbulent flame speed. The $\dot{\omega_y}$ in Equation 10 is solved using the following equations:

$$\dot{\omega_y} = A \rho_u S_t |\nabla y_{mean}| \tag{11}$$

where S_t is the turbulent flame speed which calculated using Peters correlation [18]

$$S_t = S_l(1 + \sigma_t) \tag{12}$$

$$\sigma_t = -AB + \sqrt{(AB)^2 + C\frac{u' I_l}{s_l \delta_l}} \tag{13}$$

where A,B,C are model constants, S_l is the laminar flame speed, δ_l is the laminar flame thickness, u' is the turbulence intensity, and I_t is the integral length scale. The laminar flame speed and thickness are determined using Cantera and are approximately 6.8 m/s and 0.16 mm.

To determine all chemical source terms, a skeletal mechanism developed by Luo et. al. is implemented [19]. The mechanism consists of 32 species and 206 reactions which had been reduced from the original USC detailed mechanism to include only relevant species and reactions [20]. This mechanism is selected as it contains a reasonable number of species and reactions to capture chemistry in both the finite-rate and tabulated chemistry approaches.

2.2 Problem Set-up

The inflow boundary condition with a premixed ethylene-air mixture at an equivalence ratio of 0.6 at Mach 0.6 with a turbulence intensity of 10% and integral length scale of 7 mm to match previous experiments run on the facility [10]. The pressure is set at 1.72 atm and the temperature is 1125 K. The wall boundary conditions are set to no-slip isothermal walls, with the inflow and top wall set to 800 K; the cavity walls set to 1000 K, and extender wall set to 1100 K. The side walls in the z-direction are set with periodic boundary conditions to limit the influence of confinement on the solution.

The table for the FGM solver is computed prior to the simulation to tabulate the necessary chemistry information. The ethylene-air skeletal mechanism mentioned prior is run through the 1D premixed strained flame solver at the pressure and temperature of the inflow boundary condition to approximate the reaction conditions. Since the flow is premixed, a single mixture fraction at an equivalence ratio of 0.6 is calculated. Additionally, select intermediate species are tabulated to identify the flame structure. For hydrocarbon fuels, C_2HO and OH are extracted as these are commonly measured in experimental facilities. The relevant species and temperature information in progress variable space are shown in Figure 2 to highlight their evolution through the combustion process.

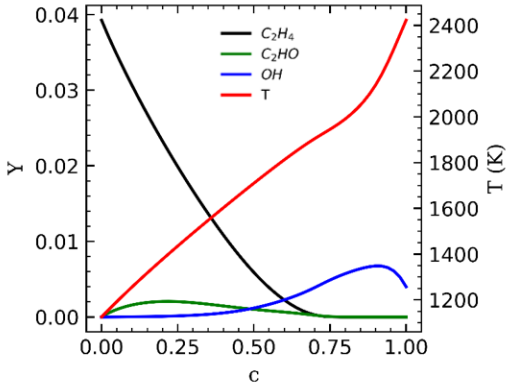

Fig. 2—Mass Fraction of C_2H_4, C_2HO, OH and Temperature as a function of normalized progress variable c

The mesh developed for these simulations consists of approximately 5 million polyhedral elements. A base element size of 500 μm is used with local refinement within the cavity and shear layer of 100 μm and 150 μm downstream of the cavity. Prism layers are used along the walls to capture boundary layer effects and sized to ensure a $Y^+ \approx 1$. The simulation is then ignited after a steady non-reacting solution is reached by imposing a high temperature region within the cavity. The solution is then run until the residuals indicate convergence has been achieved and the outflow properties have reached a nominal steady state.

3. RESULTS

3.1 Flowfield Comparison

Temperature and intermediate species are first analyzed to determine if there are any differences in the flame angle and regions of species production. Temperature and CH_2O contours are presented in Figure 3 and

4. Notable differences in the temperature distribution are present as it can be seen that the high temperature product region is more evenly distributed in the FRC case while the FGM temperature is stratified with decreasing temperature from the bottom wall to the reactants region. The peak temperature in the FGM solutions is higher and resides primarily in the cavity shear layer, reattachment region, and near the wall downstream of the cavity ramp.

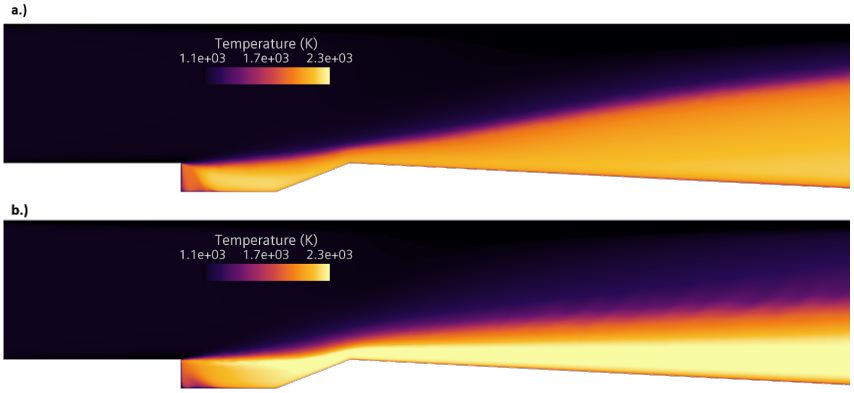

Fig. 3—Contour of Temperature for a.) FRC and b.) FGM simulations

When examining the CH_2O distribution to identify the reaction front, it is noted that the FRC contains a single small band while the FGM calculation reveals a much more diffuse distribution. Since CH_2O is commonly used experimentally to identify the flame front, these center plane contours are utilized to determine the flame angle predicted using the different chemistry solvers. Since the FGM model develops a diffuse distribution of formaldehyde production, the angle is measured from the cavity lip along the peak mass fraction band. The angle calculated for each simulation is 8.6° and 8.5°, respectively, for the FRC and FGM chemistry models.

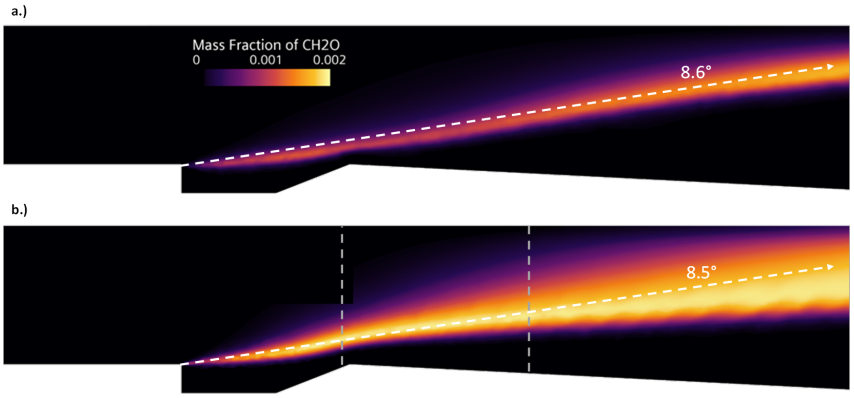

Fig. 4—Contour of Y_{CH_2O} for a.) FRC and b.) FGM simulations

Similarly, OH mass fraction center plane contours are the provided in Figure 5 as this is a commonly implemented flame diagnostic. The results indicate different regions of peak OH production, with only a thin band beginning at the cavity lip extending down stream for the FGM approach. Additionally, there is diminished OH production in the cavity when compared to the FRC. Previous numerical and experimental results have shown the flame angle measured from OH measurements to be 5.5°, which agrees well with

the FRC results. However, the FGM reveals a much shallower angle with OH production remaining closer to the combustor bottom wall. The discrepancy between the RANS simulations could be from the applied turbulence boundary condition, which results in a parabolic distribution of the turbulent kinetic energy at the cavity lip. To examine these results more closely for the species examined, profiles extracted at x = 45 mm and 65 mm (represented by the grey vertical lines in Figure 4 and 5) are provided in Figure 6. Comparing the OH profiles between the reaction methodologies, it is noted that the OH production occupies approximately the same amount of the domain and reaches similar peak values with only differences being presented in the near-wall region. Alternatively, the CH_2O production profile indicates a more significant deviation between the reaction methodologies. The peak locations of production are slightly shifted in the positive y-direction and the span of production is nearly doubled for the FGM method. Additionally, the peak magnitude of CH_2O is also doubled for FGM in comparison to FRC. The likely cause of the change in the profiles is due to the simplification of the reaction chemistry to the 1D chemistry to generate the flamelet table.

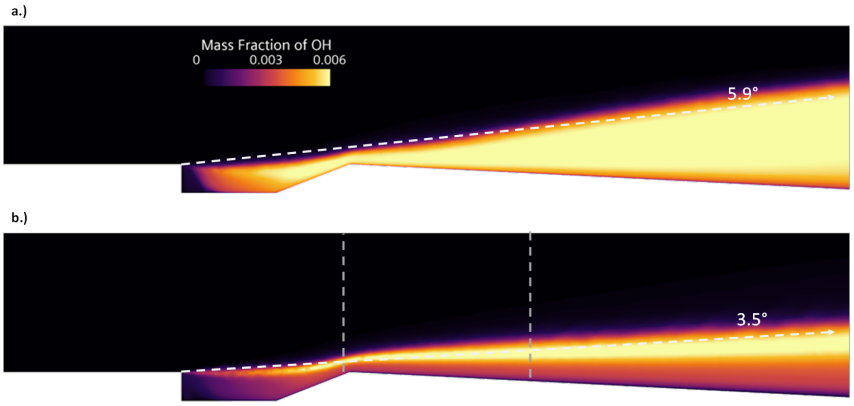

Fig. 5—Contour of Y_{OH} for a.) FRC and b.) FGM simulations

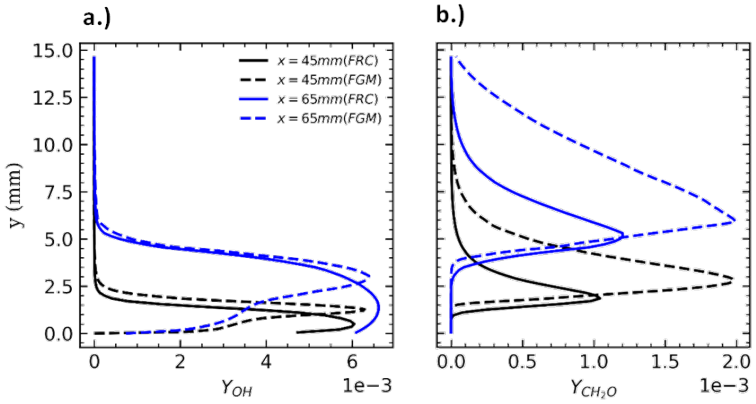

Fig. 6—a.) Y_{OH} and b.) Y_{CH_2O} profiles at x = 45 mm and x = 65 mm

To quantify the impact of the altered distribution of the combustion intermediate species on the flowfield, profiles of velocity extracted at the same locations are presented in Figure 7a. It is seen that the FGM results indicate an increase in flow velocity along the entire height of the combustor, with the most significant deviation occurring on the bottom wall of the combustor. Local heat release profiles are provided along

these profiles in Figure 7b to identify any deviations which could account for the velocity differences. The local heat release rates reveal that the FGM method predicts higher heat release rates by approximately an order of magnitude across the entire combustor height. The locations of significant deviation correspond reasonably well with the regions of velocity difference, indicating that the chemistry methodology will have some influence on the statistics extracted from the simulations.

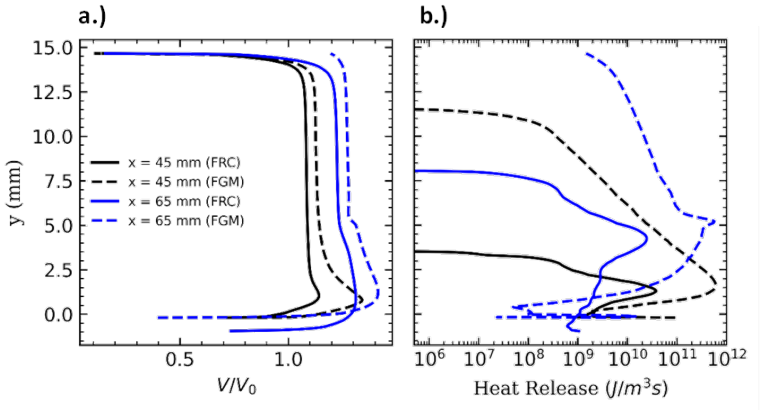

Fig. 7—a.) Velocity and b.) Heat Release profiles at x = 45 mm and x = 65 mm

As a final visualization of the flow-field, calculations of span-wise vorticity (ω_z) are presented in Figure 8 to confirm that the behavior within the cavity is not impacted by the chemistry or deviations in local heat release. The contours indicate a similar spread of the cavity shear layer, with the primary difference being a longer spread of high magnitude at the flow separation point of the cavity shear layer. The formation of the secondary vortex near the front wall of the cavity is slightly suppressed in the FGM simulation.

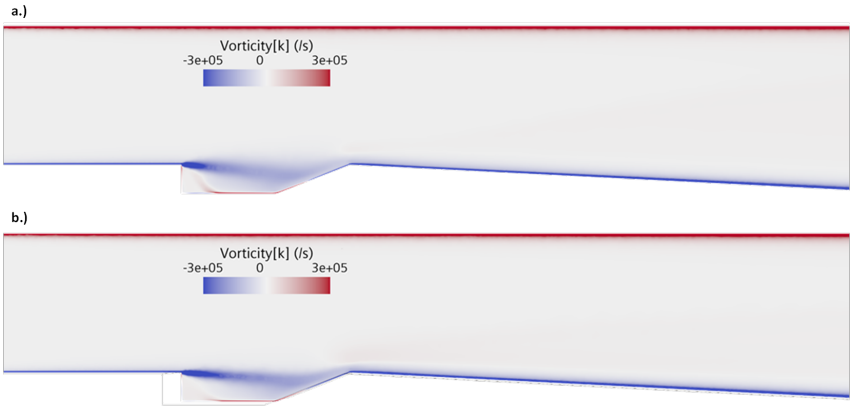

Fig. 8—Contour of ω_z for a.) FRC and b.) FGM simulations

3.2 Combustor Outflow Properties

In some cases, the desired analysis may only require knowledge of the outflow conditions of the combustor to aid in calculating thrust, specific impulse, etc. To determine any influence the reacting flow methodology has on the outflow characteristics, the average temperature, pressure, and velocity are determined at the outflow plane and presented in Table 1. The percent difference is taken with respect to the FRC method as it

directly solves the species transport equation and does not rely on tabulated chemistry. The results indicate that for all properties there is an approximate 5-7% difference in the FGM solution when compared to the FRC results. The temperature difference between the methods can be accounted for the stratified temperature profile shown previously in Figure 3 where a larger portion of the outflow is at a lower temperature. Correspondingly, the lower temperature results in a lower density, which accounts for the decrease in velocity.

Model	Temperature (K)	Pressure (kPa)	Velocity (m/s)
FRC	1877	177	515
FGM	1781	187	482
% Difference	5.08	5.80	6.80

Table 1—Combustor outflow conditions for FRC and FGM simulations

3.3 Computational Cost

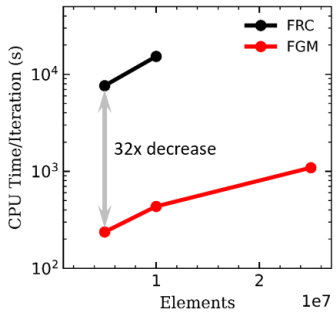

Fig. 9—CPU time/iteration for FRC and FGM simulations

The computational expense of the two chemistry modeling approaches is significantly different, especially when considering large mechanisms which contain a significant number of reactions and species. The CPU time required for each approach is monitored and presented in Figure 9 for both methodologies and different mesh sizes. The results indicate that there is an approximately 32x decrease in the CPU time required per iteration for the FGM method on the same grid. The 32x decrease is directly proportional to the number of species in the chemical mechanism used to model the ethylene-air reaction. As a simulation can take thousands of iterations to achieve convergence, the cost savings become very significant over the course of an entire simulation. Therefore this indicates that if only bulk properties (e.g. pressure, velocity, temperature) are desired and not local flame front statistics (Intermediate Species, Temperature distributions) the FGM method provides a more cost-effective solution. As shown previously in Table 1 a 5-7% error would still provide a reasonable approximation for engine performance statistics.

4. CONCLUSIONS

Three-dimensional Reynolds Averaged Navier-Stokes simulations were performed on the University of Virginia Supersonic Combustion Facility to determine the influence of the chemistry modeling approach on the results. The facility was simulated using a premixed ethylene-air mixture with an equivalence ratio of

0.6. The inflow was set at conditions of Mach 0.6 with a turbulence intensity of 10%. The ethylene-air combustion model is solved using finite-rate chemistry and a flamelet generated manifold approach using a 32 species, 206 reaction skeletal mechanism.

The results of the FRC and FGM are compared to quantify differences in the results and computational expense. The simulation results have general agreement for the flame angle; however, when examining the intermediate species there are discrepancies that arise. In the case of CH_2O, the FGM model predicts a more diffuse spread of formaldehyde production. Since formaldehyde is typically used as a flame front marker, the FRC provides a more accurate prediction of the flame front location. However, the OH distribution shows general agreement between the two models, with only primary differences being the near the combustor bottom walls. The velocity profiles and local heat release profiles are examined and it is shown that the FGM method provides higher velocity which is determined to be linked to higher local heat release rates within these regions.

Statistics from the outflow of the combustor are extracted and compared for each modeling method. The results indicated that their is a 5-7% difference between for the FGM method when considering the temperature, pressure, and velocity. The computation time is then compared between each method and it is shown that there is an approximately 32x decrease in CPU time/iteration when using the FGM method as opposed to FRC. This indicates that using the FGM methodology provides a more cost-effective option when the primary concern of the analysis is global statistics for measuring thrust or other similar metrics. However, if local flame front behavior is the primary concern of the analysis on the combustor, the FRC approach is more appropriate.

ACKNOWLEDGMENTS

The authors would like to acknowledge the support of the Base Program at the Naval Research Laboratory.

REFERENCES

1. C. Segal, *The Scramjet Engine: Processes and Characteristics*, Cambridge Aerospace Series (Cambridge University Press, 2009).

2. M. R. Gruber, J. M. Donbar, C. D. Carter, and K. Y. Hsu, "Mixing and Combustion Studies Using Cavity-Based Flameholders in a Supersonic Flow," *Journal of Propulsion and Power* **20**(5), 769–778 (2004).

3. F. W. Barnes and C. Segal, "Cavity-based flameholding for chemically-reacting supersonic flows," *Progress in Aerospace Sciences* **76**, 24–41 (2015).

4. C. C. Rasmussen, J. F. Driscoll, K. Y. Hsu, J. M. Donbar, M. R. Gruber, and C. D. Carter, "Stability limits of cavity-stabilized flames in supersonic flow," *Proceedings of the Combustion Institute* **30**(2), 2825–2833 (2005).

5. H. Wang, Z. Wang, M. Sun, and N. Qin, "Combustion characteristics in a supersonic combustor with hydrogen injection upstream of cavity flameholder," *Proceedings of the Combustion Institute* **34**(2), 2073–2082 (2013).

6. J. W. Kirik, C. P. Goyne, J. C. McDaniel, R. D. Rockwell, L. M. Cantu, E. C. Gallo, and A. D. Cutler, "Aerodynamic characterization of a cavity flameholder in a premixed dual-mode scramjet," *Journal of Propulsion and Power* **34**(3), 739–749 (2018).

7. A. D. Cutler, E. C. Gallo, L. M. Cantu, R. D. Rockwell, and C. P. Goyne, "Coherent anti-Stokes Raman spectroscopy of a premixed ethylene–air flame in a dual-mode scramjet," *Combustion and Flame* **189**, 92–105 (2018).

8. A. S. Potturi and J. R. Edwards, "Large-eddy/Reynolds-averaged Navier–Stokes simulation of cavity-stabilized ethylene combustion," *Combustion and Flame* **162**(4), 1176–1192 (2015).

9. T. Nielsen, J. R. Edwards, H. K. Chelliah, D. Lieber, C. P. Goyne, R. D. Rockwell, and A. D. Cutler, "Hybrid LES/RANS simulation of supersonic premixed ethylene combustion," Proceedings of the 2018 AIAA Aerospace Sciences Meeting, 2018, p. 1145.

10. T. B. Nielsen, J. R. Edwards, H. K. Chelliah, D. Lieber, C. Geipel, C. P. Goyne, R. D. Rockwell, and A. D. Cutler, "Hybrid Large Eddy Simulation/Reynolds-Averaged Navier–Stokes Analysis of a Premixed Ethylene-Fueled Dual-Mode Scramjet Combustor," *AIAA Journal* **59**(7), 2440–2456 (2021).

11. G. B. Goodwin, R. F. Johnson, D. Kessler, and H. K. Chelliah, "Premixed ethylene-air combustion in a dual-mode scramjet cavity combustor with a turbulent inflow," Proceedings of the AIAA Propulsion and Energy 2019 Forum, 2019, p. 4270.

12. R. F. Johnson, G. B. Goodwin, A. T. Corrigan, A. Kercher, and H. K. Chelliah, "Discontinuous-Galerkin Simulations of Premixed Ethylene-Air Combustion in a Cavity Combustor," Proceedings of the AIAA Scitech 2019 Forum, 2019, p. 1444.

13. G. B. Goodwin, R. F. Johnson, D. A. Kessler, A. D. Kercher, and H. K. Chelliah, "Effect of Inflow Turbulence on Premixed Combustion in a Cavity Flameholder," *arXiv preprint arXiv:2001.05893* (2020).

14. F. R. Menter, "Two-equation eddy-viscosity turbulence models for engineering applications," *AIAA Journal* **32**(8), 1598–1605 (1994).

15. J. R. Edwards and J. A. Fulton, "Development of a RANS and LES/RANS Flow Solver for High-Speed Engine Flowpath Simulations," Proceedings of the 20th AIAA International Space Planes and Hypersonic Systems and Technologies Conference, 2015.

16. E. Hassan, D. M. Peterson, D. K. Walters, and E. A. Luke, "Dynamic Hybrid Reynolds-Averaged Navier–Stokes/Large-Eddy Simulation of a Supersonic Cavity: Chemistry Effects," *Journal of Propulsion and Power* **35**(1), 201–212 (2019).

17. T. Roos, A. Pudsey, M. Bricalli, and H. Ogawa, "Cavity enhanced jet interactions in a scramjet combustor," *Acta Astronautica* **157**, 162–179 (2019).

18. N. Peters, *Turbulent Combustion* (Cambridge University Press, 2000).

19. Z. Luo, C. S. Yoo, E. S. Richardson, J. H. Chen, C. K. Law, and T. Lu, "Chemical explosive mode analysis for a turbulent lifted ethylene jet flame in highly-heated coflow," *Combustion and Flame* **159**(1), 265–274 (2012).

20. H. Wang and A. Laskin, "A comprehensive kinetic model of ethylene and acetylene oxidation at high temperatures," *Progress report for an AFOSR new world vista program* (1998).